CHAPTER 12. SURFACE STRUCTURES OF GOLD AND GOLD-BASED BIMETALLIC NANOPARTICLES

S. SHAIKHUTDINOV

Department of Chemical Physics, Fritz Haber Institute of the Max Planck Society, Faradayweg 4-6, Berlin 14195, Germany

12.1. Introduction

Since Roman times it has been recognized that gold dispersed in glasses gives rise to fascinating optical phenomena, which were (much later, of course) rationalized on the basis of *physical* properties of gold in highly dispersed state (see Chapter 2). Regarding its *chemical* properties, gold has long been considered as an inert material since bulk gold does not react easily with many molecules typically present in the ambient atmosphere, the property that renders gold the most noble metal. Chemistry of gold has only recently received much attention after superior catalytic properties observed for highly dispersed gold in a number of industrially important reactions such as low temperature CO oxidation, selective oxidation of propene, water gas shift reaction, selective hydrogenation of acetylene, to name a few. (refs. [1-5], see also Chapter 9). Obviously, the performance of gold in heterogeneous catalysts is primarily determined by geometrical and electronic structures of gold species which are *surface* in nature. The surface structures become very complex in the case of nano-sized gold particles, which expose facets of different orientations as well as substantial amounts of undercoordinated atoms. The issue becomes even more complicated in the presence of a support (typically, an oxide with the high surface area), which may not necessarily behave as an inert "spectator", but rather as a key player which controls reactivity of gold, for example, through stabilization of particular structures of gold species and gold/support interface.

The atomic-level understanding of structure, composition and electronic state of surfaces can only be obtained by surface-sensitive techniques, which are commonly employed in Surface Science. The recent surge in study of gold catalysts, [1-5] has been accompanied by a corresponding swell of interest in the surface science of gold. In spite

of the enhanced activities worldwide, the surface chemistry of the small gold particles is still far from being well-understood at the atomic scale. Partially, this is due to the fact that the real catalytic systems, consisting of Au nanoparticles deposited on oxide supports with poorly-defined surface structures, are too complex for making precise and unambiguous structural characterization of such systems which may, in turn, be linked to their functional properties. This renders careful model studies a necessity. Within the so-called "surface science" approach,[6-16] the structural complexity of a real catalyst is reduced to a well-defined model. The latter, however, should retain the main features of the real system such as nature of a support, high dispersion of a supported metal, etc.

Numerous surface science studies are currently being performed in order to understand the fundamental aspects of catalysis by gold, in particular addressing the key question: why gold behaves as a catalyst when its dimensions are reduced to the nanometer scale (see, for instance, reviews [16-23]).

The Chapter will focus on surface structures of gold nanoparticles deposited on well-defined planar oxide supports. A number of model systems will be discussed here in order to illustrate the approach to surface chemistry of gold and also to demonstrate the complexity of the gold/support interaction. After description of model systems in Section 12.2, we will briefly discuss surface structures of gold single crystals (Section 12.3). Basic structural motifs of Au nanoparticles are discussed in Section 12.4. The preparation of thin film supports will be addressed in Section 12.5. Then in Section 12.6, we show basic principles of gold deposition onto planar supports. Section 12.7 presents case studies of size, support end environmental effects observed on Au/oxide model systems. Then we address supported gold species in the form of single-layer islands which represent gold in a two-dimensional state causing certain differences as compared to a three-dimensional counterpart (Section 12.7). Finally, effects of gold alloying with other metals will be discussed in Section 12.8.

Certainly, this Chapter is not aimed at providing a comprehensive review of the current studies on surface science of gold. It rather demonstrates opportunities and limitations of the approach towards deeper understanding of surface chemistry of gold in highly dispersed state.

12.2. Background

In planar model systems metal particles are deposited onto an electrically conducting oxide single crystal or a thin metal-oxide film grown on a metal single crystal substrate as schematically shown in Fig. 12.1. The system allows the facile application of a large variety of surface sensitive techniques for precise system characterization such as:

- Electron spectroscopy, e.g., Ultraviolet and X-ray Photoelectron Spectroscopy (UPS/XPS), in particular using the synchrotron light source, and Auger Electron Spectroscopy (AES). The methods allow to determine the elemental surface composition, the oxidation states of the constituting elements, and the valence band structure.
- Ion spectroscopy, e.g., Low Energy Ion Surface Scattering (LEISS) and Secondary Ion Mass-Spectrometry (SIMS). The methods provide information on the composition of the topmost surface layers in combination with an elemental depth-profile analysis upon surface sputtering.
- Vibrational spectroscopy, e.g., High Resolution Electron Energy Loss Spectroscopy (HREELS), and Infrared Reflection-Absorption Spectroscopy (IRAS). The methods monitor the lattice vibrations (phonons) and also the vibrations of adsorbed species.
- Low Energy Electron Diffraction (LEED), Surface X-ray Diffraction (SXRD) and Grazing Incident Small Angle X-ray Scattering (GISAXS). The methods are usually employed for ordered structures and interfaces.
- Scanning probe microscopy, e.g., Scanning Tunneling Microscopy (STM), and Atomic Force Microscopy (AFM). These seem to be only methods which allow to determine morphology (topography) of the surface nanostructures with atomic resolution.

In addition to the above techniques, adsorption and reaction of molecules on these surfaces can readily be studied by Temperature Programmed Desorption (TPD) as the planar systems do not suffer from diffusion limitations existing for powdered and microporous materials. Kinetics and elementary steps of chemical reactions at surfaces

can be monitored by Molecular Beam technique, particularly in combination with IRAS (see, for example, the review [24]).

Although most of the surface sensitive techniques can only be applied in high and ultra-high vacuum (UHV), while catalytic processes occur at ambient pressures, *in situ* methods have been developed to bridge the so-called "pressure gap". Sum Frequency Generation (SFG), Polarization-Modulation IRAS (PM IRAS), Ambient-Pressure XPS (AP XPS) and High-Pressure STM techniques allow one to carry out studies at more realistic pressure conditions. [25-30] Furthermore, *in situ* structural characterisation can be performed simultaneously with reactivity measurements using gas chromatography, in essence, in the same way as it is routinely used in catalytic experiments.

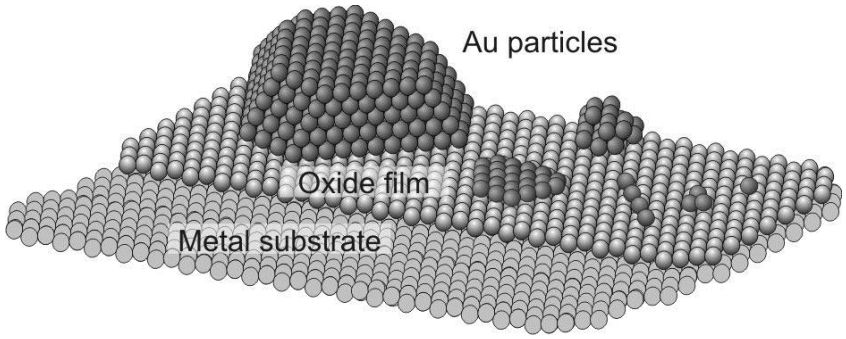

Figure 12.1. Model planar systems for studying surface structures and reactivity of gold nanoparticles supported on well-defined thin oxide films.

Basically, a research strategy of model "surface science" studies includes the following "elementary" steps:

- Preparation of a planar support and its characterization with respect to morphology, surface composition, and structural defects;
- Deposition of metal particles onto the support and monitoring the nucleation and growth process;
- Structural characterization of the supported metal particles, in particular their size, shape, electronic state, and thermal stability;

- Adsorption studies of molecules participating in a target catalytic reaction as well as of the "probe" molecules, adsorption of which is sensitive to the surface structure;
- Reactivity studies under nearly realistic conditions to establish reaction kinetics as a function of the gas composition and temperature;

Structure-reactivity relationships, such as size, support, and environmental effects, observed from such experiments provide important, if not crucial information for understanding surface chemistry of metal nanoparticles and elucidating reaction mechanisms.

12.3. Surface Structures of Gold Single Crystals

Although the catalytic nature of gold is most likely linked to size and structure issues, it is instructive here to address first the atomic structures of gold single crystal surfaces. In addition, the extended surfaces are well suited for studying surface reconstructions, if any, which may occur under reaction conditions.

Gold shares a face centred cubic (*fcc*) lattice. The low Miller indexed surfaces of gold, such as (111), (110) and (100), shown in Fig. 12.2, are all known to undergo surface reconstruction in UHV. Perhaps, the most famous and still intriguing is the reconstruction of the Au(111) surface, unique for pure *fcc* metals, which is referred to as a "herringbone" reconstruction after first atomically resolved STM images [31] (see Fig. 12.3a). The reconstruction can be described by a complex stacking-fault-domain model of the topmost layer having higher surface density of atoms than in the bulk layers [31-33] and rationalized in terms of surface states that arise due to the interaction of *sp* and *d* states, a consequence of its relativistic nature.[34] (See Chapter 2).

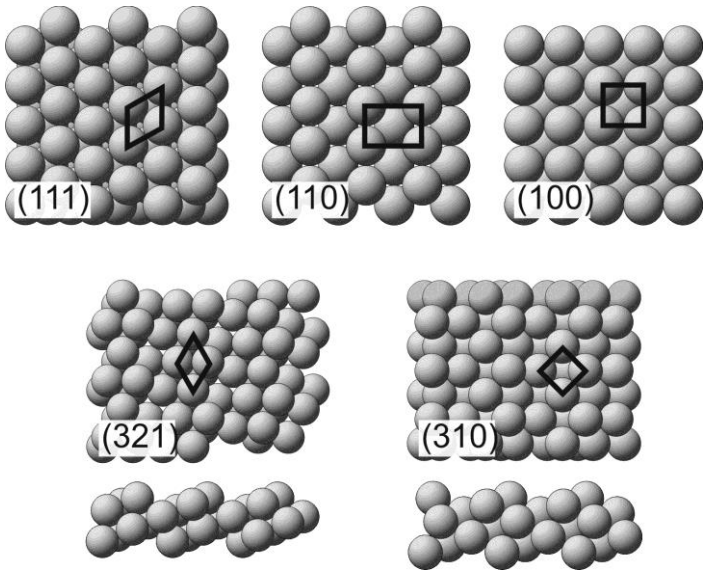

Figure 12.2. (Top panel) Top views of unreconstructed (111), (110) and (100) surfaces of fcc metals. The unit cells are indicated. (Bottom panel) Top and cross views of the stepped Au(321) and Au(310) surfaces. The (111) and (100) unit cells of the microfacets are indicated.

The Au(110) surface reconstructs into the (1×2) surface which is formed by "missing rows" along [1-10] direction as shown in inset in Fig. 12.3b.[35] This reconstruction gives rise to three different types of surface atoms: on top of row, side of row, and trench atoms. The sides of row atoms are arranged in the same manner as the (111) surface and often referred to as (111) microfacets.

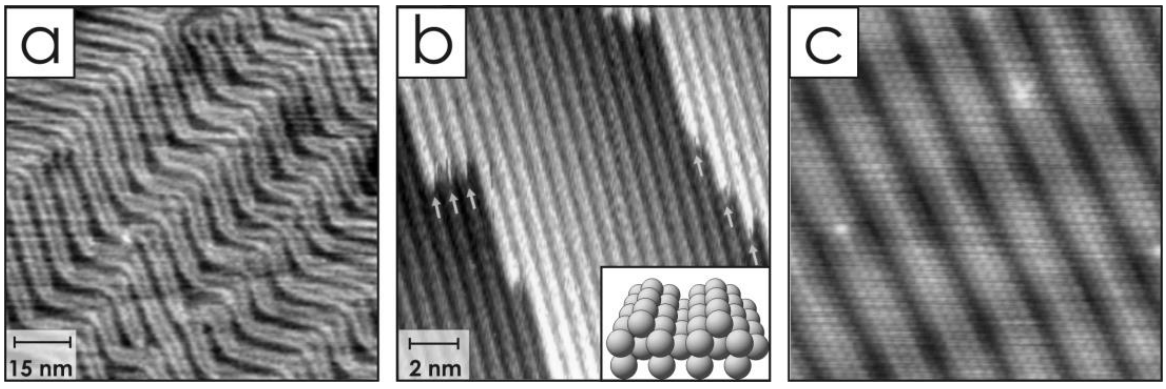

Figure 12.3. STM images of (a) the "herringbone" reconstruction of Au(111); (b) the (1x2) "missing row" reconstruction of Au(110) (adapted from ref. [35]. Copyright (1992) by the

American Physical Society); (c) the “hexagonal” reconstruction of Au(100) (reproduced from [36])

The reconstruction of the Au(100) surface apparently depends on preparation and remains controversial. It has originally been assigned to (1×5) “adding row” reconstruction. [37] Later, more complex surface structures have been observed (see Fig. 12.3c), such as (5×20),[38] a (5x20) with rotation,[39] a hexagonal (28×5)R0.6°,[40] to name a few.

It has been proposed that the reconstructed surfaces may experience different combinations of these structures depending upon step density and surface temperature.[41] The reconstruction is generally believed to be limited to the first layer, thus indicating that the more compact surface arrangement is favored to a degree where the energy cost due to a lack of commensuration with the layer underneath can be overcome.[42]

These reconstructions of the gold surfaces are quite stable under vacuum conditions. For example, the herringbone reconstruction of Au(111) was seen at ~ 850 K,[43] but can be lifted upon adsorption of certain gases such as CO. SXRD studies [44] revealed lattice expansion of the Au(111) surface exposed to CO at 300 K at pressures between 0.1 and 530 mbar, although the herringbone reconstruction was preserved. Even more extensive surface transformations of Au(111) were observed upon exposure to 110 mbar CO at 600 K. Similar behavior was found for Au(110) at CO pressures above 0.1 mbar. [45] STM results showed significant surface roughening and a lifting of terrace anisotropy. Since the morphological changes observed for both, Au(111) and Au(110) surfaces were remained after evacuation, CO dissociation might have occurred at high pressures accompanied by carbon deposition.

A limited number of studies were reported on gold single crystal surfaces with higher Miller indexes, e.g., Au (991), Au(430), Au(221), Au(332), Au(310) and Au(321).[46-48] The latter two surfaces are shown in Fig. 12.2. The (321) surface forms (111) microfacets, whereas the (310) surface exhibits (100)-like facets, with the step atoms on both surfaces having a coordination number 6. Comparison of adsorption properties of CO (which is very often used for the characterization of the gold-based

catalysts) on the two surfaces revealed that CO binding to gold is not only dependent of the coordination number but the exact geometrical surface structure.[48] The studies on the stepped Au surfaces are helpful for understanding the reactivity of the low-coordinated gold atoms, which become dominating the surfaces of gold nanoparticles.

12.4. Morphology of Gold Nanoparticles: General Considerations

In principle, small metal particles expose different facets resulted from a truncation of single crystals. In principle, the surface energies of (*hkl*) planes, described as the Gibbs free energy per unit area, determine the morphology of particles. Having obtained the free energies of the single crystal surfaces (γ_{hkl}), one can predict an equilibrium crystal shape of an unsupported particle (in the same environment as single crystal surfaces) for a given volume using the so-called Wulff construction. [49-51] Representing the surface free energy as a function of direction by vectors of length γ_{hkl} the minimum energy shape at a constant volume is the inner envelope of the normals to this surface (see Fig. 12.4).

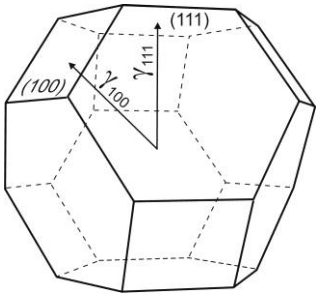

Figure 12.4. The Wulff construction of (fcc) metal polyhedral particles comprising (111) and (100) faces.

Beyond the truncated octahedron, shown in Fig. 4, and their twinned variants, the possible structures include also decahedral and icosahedral motifs,[51-53] as schematically shown in Fig. 12.5. The latter structures have a relatively high strain energy.[54]

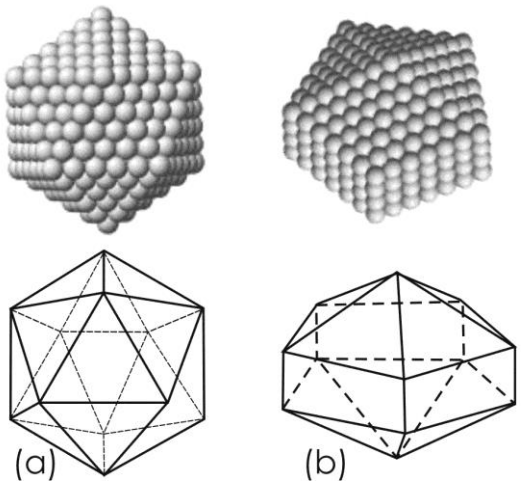

Figure 12.5. Icosahedral (a) and decahedral (b) structures of gold nanoparticles.

Obviously, the above described thermodynamic approach is valid only for a particle that reached an equilibrium shape. Note also, that this construction neglects any contribution of "edge" and "corner" sites and can, therefore, be applied only to relatively large particles, where the facet dimensions are much larger than the surface unit cells. Basically, metal particles at moderate sizes (several tens of nanometers) are generally consistent with the Wulff construction.[51] The situation becomes more complicated upon reducing the size down to several nanometers. Surface stress, size dependent lattice parameter changes, twin boundaries, and ambient conditions, all these factors may influence the morphology of metal particles.[51] For supported particles, the role of substrate may be included in the construction by replacing the free surface energy of the contact plane with an effective surface energy (γ^*) which is the difference between the interface energy and the surface energy of the substrate:[50]

$$\gamma^* = \gamma_{interface} - \gamma_{support} \quad (1)$$

This gives the equilibrium shape truncated at the interface (see Fig. 12.6):[11]

$$\Delta h/h_i = W_{adh} / \gamma_{metal(i)} \quad (2)$$

where W_{adh} is the adhesion energy, which is defined as the energy per unit area to pull the system apart to its constituents, and relates to the surface energies through the equation:

$$W_{adh} = \gamma_{metal(i)} + \gamma_{support} - \gamma_{interface} = \gamma_{metal(i)} - \gamma^* \qquad (3)$$

It is evident from (2) and (3) that, for negative values of γ^*, the particle height becomes smaller than the corresponding radii of the unsupported particle. Clearly, the higher the adhesion energy, the more flattened the particle is. Therefore, flattening of metal particles may be considered as the physical manifestation of the strong metal-support interaction.

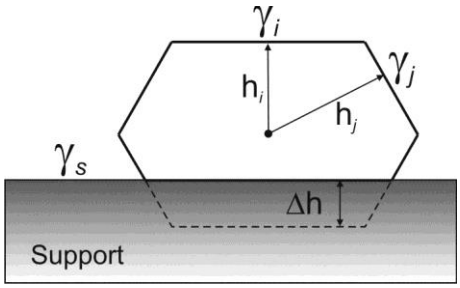

Figure 12.6. Schematic representation of the Wulff construction for supported particles (see text).

High resolution transmission electron microscopy (HRTEM) studies revealed that the structure of very small Au nanoparticles (d ~ 1 nm) fluctuated significantly even at room temperature (the phenomenon was later referred to as "quasimelting" [51,55,56]), as the energy difference between conformations calculated for gas phase clusters is comparable with kT. [55] Although several effects may contribute to this phenomenon including an electron beam induced overheating, it appears that the substrate plays a critical role in the stabilization of the particle in particular states. Indeed, the lack of such structural transitions on Au deposited onto vacuum-cleaved MgO microcubes was explained by the high interfacial energy which must be overcome when the particles are epitaxially oriented to the support.[57] Also *in situ* HRTEM monitoring [58] of a gold single particle, growing on a MgO(100) step while continuous gold deposition in

vacuum, revealed that the particle rearranged continuously, apparently to maintain the lowest energy structure. Shape modulation from tetragonal pyramid to truncated tetragonal pyramid or the inverse was observed repeatedly. Examining the surface area ratios of Au(100) and Au(111) facets during the particle growth, repetitions in the truncation pattern were seen to emerge as the cluster grew until reaching a size of over 1400 atoms. It should be mentioned, however, that the kinetics of particle growth may also affect the resulting morphology of deposited Au nanoparticles (see below).

Atomic-scale imaging of metal particles has been substantially improved by using aberration-corrected scanning transmission electron microscopy (ac-STEM).[59] In particular, in the case of Au/MgO system discussed above, STEM studies revealed semicoherent interfacial epitaxy and coordinate-dependent surface contraction for the fcc (001) oriented Au nanoparticles (2–3 nm in diameter), suggesting that their interaction with the substrate is relatively weak. In addition, a significant change in interfacial separation distance from 2.47 ± 0.12 Å for the fcc (001) oriented Au nanoparticles to 3.07 ± 0.11 Å for the fcc (111) oriented Au nanoparticles has been observed.[60]

12.5. Planar Supports

Following the research strategy presented in Section 12.2, the first step in the preparation of supported gold model systems is the fabrication of a planar support with a well-defined structure. Among those, oxide single crystals, such as MgO, TiO_2, sapphire (Al_2O_3), quartz (SiO_2), were of first choice in early studies.[11,16] However, the lack of electrical conductivity (most oxides are wide gap semiconductors or insulators) renders their use for surface-science studies very difficult, except the partially reduced forms of rutile TiO_2(110) crystal which seems to be the most widely studied support used for gold model catalysts. In contrast, thin oxide films grown on metal single crystals provide good electrical and thermal conductivity for a facile application of surface science techniques. In addition, the surface selection rules [61] (i.e., only vibrations with dipole moment changes normal to the metal surface can be detected by IRAS) often ease assignment of infra-red bands.

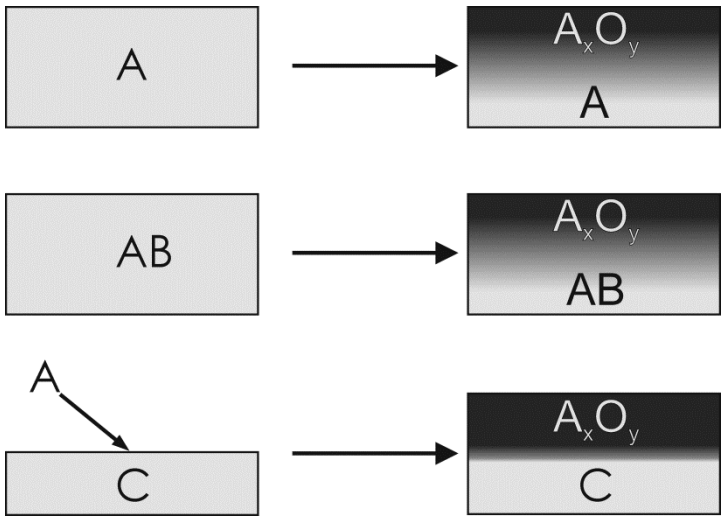

Figure 12.7. Preparations of well-ordered thin oxide films by oxidation of a metal single crystal (top), by oxidation of bimetallic surfaces (middle), and by deposition/oxidation of metal overlayer on the second metal single crystal (bottom).

Various methods for preparation of thin oxide films are reported in the literature, see reviews [8,9,13,62,63]. The first one is the direct oxidation of a metal single crystal as schematically shown in Fig. 12.7. However, this preparation primarily results in amorphous or polycrystalline overlayers (*e.g.*, SiO_2/Si, Al_2O_3/Al)[64,65] or crystalline films with a high density of defects (e.g., NiO(100)/Ni(100).[66] Formation of a crystalline Cr_2O_3(111) film on Cr(110) appears as the only successful example for such preparation.[67]

Another route is the oxidation of bimetallic or alloyed surfaces where the element having higher affinity for oxygen segregates to the surface and becomes oxidized, ultimately forming thin oxide film at elevated temperatures. Perhaps, the best examples of the crystalline films fabricated using this approach are the alumina ultrathin films grown on NiAl(110), NiAl(111) and Ni_3Al(111) single crystals. [13,68-70]

In great majority of cases, however, oxide films are prepared by vapor deposition of one metal (to be oxidized) onto the second metal (usually, noble metal) single crystal either in oxygen ambient or in vacuum followed by post-annealing in vacuum or in oxygen, respectively. In addition, a metal substrate can be pre-covered with atomic oxygen to ease oxidation of incoming metal atoms and to prevent their migration into the

substrate bulk. Numerous oxide films were grown in this way, such as Fe_3O_4(111) and Fe_2O_3(0001) films on Pt(111), [63] MgO(001)/Ag(001), [71] CeO_2(111)/Ru(0001), [72,73] V_2O_3(0001)/Pd(111), [74] V_2O_5(001)/Au(111), [75] SiO_2/Ru(0001), [76] to name a few.

It is noteworthy that highly oriented pyrolytic graphite (HOPG) has also been used as a planar substrate for gold nanoparticles due to its flatness and good electrical conductivity. However, graphite only shows a weak interaction with gold, thus resulting in relatively large Au particles even at room temperature.[77] To some extent, the gold particle density and size can be varied by ion sputtering and/or oxidation which result in etched pits on the HOPG surface, which, in turn, serve as nucleation centers for diffusing gold ad-atoms. [23,77]

12.6. Gold Deposition on Planar Supports

12.6.1 Physical vapor deposition

Most commonly gold particles are deposited onto planar oxide supports in vacuum using *Physical Vapor Deposition* (PVD), which provides the best cleanliness of the systems under study. There are various realizations of PVD depending on how a metal vapor is produced, e.g. by thermal evaporation, by sputtering of metal target using high energy ions, by laser ablation, etc (see below).

For the thermal evaporation, gold is placed into a crucible (usually made of high melting point materials such as W and Mo) that is heated resistively or using electron beam (see Fig. 12.8). Since gold has a relatively high vapor pressure, the reasonable flux can be obtained at the temperatures close to or just above the melting point of gold (1337 K). The most simple, "home-built" evaporators can be made of a gold wire wrapped around tungsten wire, which is heated by passing the electric current to first form a small droplet of gold. The deposition flux of gold atoms from these sources is typically in the range of 10^{14} atoms cm^{-2} sec^{-1}, which can be measured either by a quartz microbalance or directly by STM using the support on which Au atoms adsorb with a high sticking coefficient.

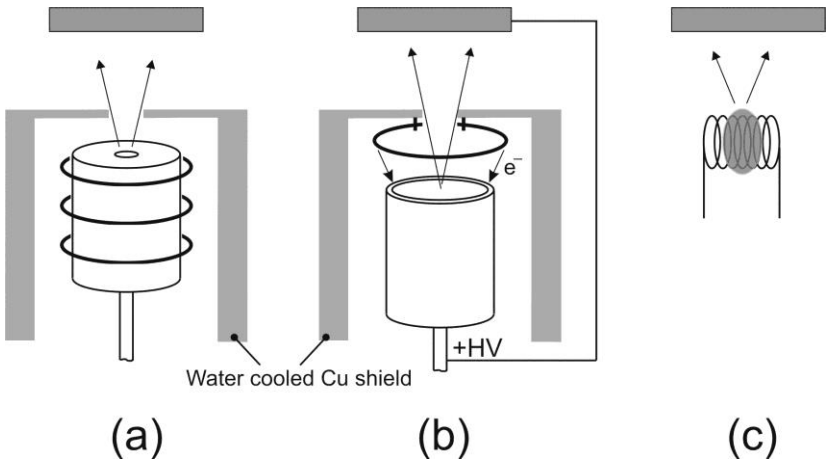

Figure 12.8. PVD sources commonly used for gold deposition on planar supports. A crucible filled with metallic gold is heated resistively (a) or by electron bombardment (b). In (b) the substrate is biased at the same high voltage potential as the crucible (typically 800 - 1000 V) to prevent accelerating of charged gold species towards the substrate. Evaporators have normally a water-cooled Cu shield to maintain the UHV conditions during the deposition. (c) The "home-built" evaporator consisting of tungsten filament with a small Au droplet formed upon resistive heating of the Au wire wrapped around the tungsten filament.

Note, that other recently developed PVD methods include a glow plasma discharge or a cathodic arc to vaporize the target material. In the pulsed laser deposition method, a high power laser ablates material from the target into a vapor. Although the experimental set-up may be fairly simple, the ablation process itself is extremely complex involving the interaction between the laser and a solid target material, plasma formation and the transport of material across the vacuum to the substrate. All these methods are rarely used for PVD of pure metals like gold, but rather for multi-elemental compounds and materials with low vapor pressures.

From any deposition source, the incoming Au atoms first adsorb onto the surface, then diffuse and ultimately aggregate into clusters and nanoparticles as schematically shown in Fig. 12.9. In principle, two types of nucleation modes may occur at surfaces: homogeneous and heterogeneous. For the *homogeneous nucleation*, an immobile nucleus is formed on regular surface sites by aggregation of several atoms. The critical island size

is defined as the size above which the islands are stable. In other words, by addition of further atoms, the nuclei will grow, whereas islands up to this size can dissolve again. For the simplest situation, when a dimer is already stable species (the critical size is one atom), theoretical considerations show [9,78] that the saturation density of islands N depends on the diffusion coefficient D and the deposition flux F as $N \sim (F/D)^{1/3}$. Then no further nuclei form, and all diffusing atoms stick to existing islands. (For more sophisticated analysis the readers refer to the ref. [9] and references therein).

However, if defects are present on the surface, the ad-atoms may be trapped at these sites, thus forming nucleation centers for subsequent growth, which is called *heterogeneous nucleation*. If the interaction of ad-atoms with defects is strong and the defect density is relatively high, the metal particle density will be independent of the deposition flux. (It is important to note here that, using electron beam assisted evaporators and other methods resulting in high-energy charged species (typically, 500 - 1000 eV), one needs to take precautions against accelerating of the ionized metal atoms towards a substrate, which may create additional defects upon collision as nucleation centers for subsequent gold particles. Although there are no yet systematic studies on this effect, it is strongly recommended to bias the support, at least, at the same potential as the metal source, see Fig. 12.8b).

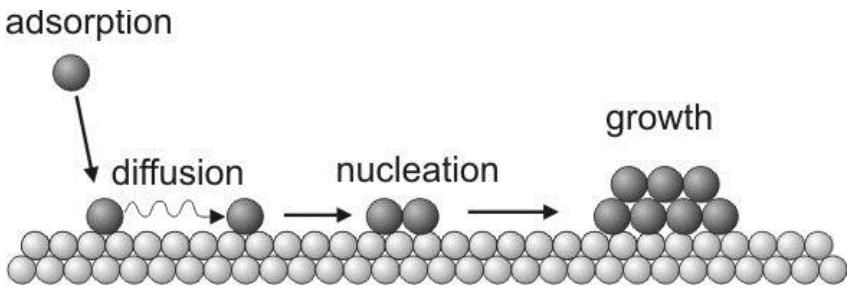

Figure 12.9. Elementary steps of the formation of Au particles by physical vapor deposition.

The nucleation and growth of gold deposited by PVD on oxide supports is often governed by the defect structure of the support (i.e., point defects (for example, oxygen vacancies), step edges, impurities) as a result of relatively weak interaction of gold with

oxides and hence high surface diffusivity of gold ad-atoms. Such effect may even be used for decorating surface defects to count them.[73]

Certainly, the substrate temperature can alter the growth processes. Indeed, the Au ad-atoms may escape from defect sites at elevated temperatures and keep on diffusing across the surface. In addition, the particles usually sinter and/or coalesce at high temperatures. Very often, the size and the shape of the gold aggregates formed at low temperatures is kinetically limited as illustrated in Fig. 12.10 for Au deposited on the Fe_3O_4(111) films. When deposited at ~ 100 K, the Au particles exhibit a broad size distribution and poorly-defined (irregular) shape, whereas the annealed at 500 K system exposes well-faceted particles with a more uniform particle size distribution.

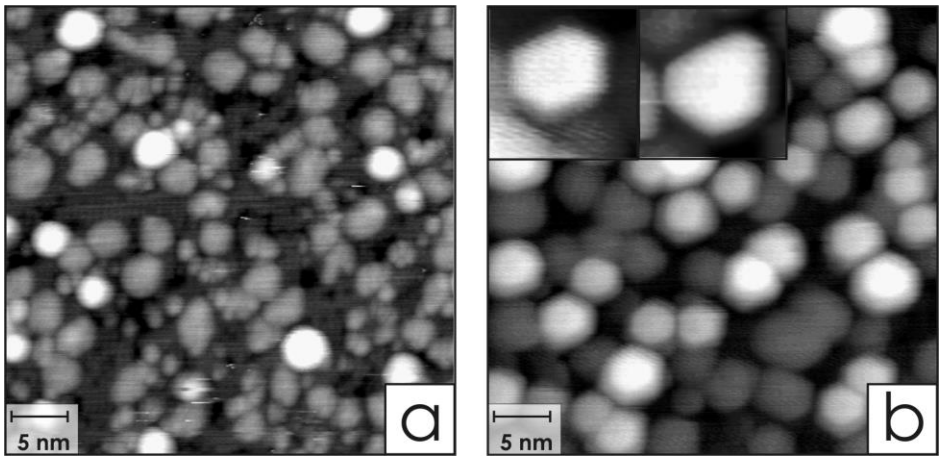

Figure 12.10. Typical STM images of Au particles deposited by PVD on a Fe_3O_4(111) film at 100 K (a) and after annealing to 500 K (b). The characteristic shapes of the annealed Au particles are shown in the inset.

In principle, a range of particle sizes between 1 and 10 nm can readily be prepared by PVD. A degree of size control can be achieved by optimizing the coverage, substrate temperature and deposition flux.

12.6.2. Cluster deposition

In the range of very small sizes, a "soft-landing" of *mass-selected clusters* pre-formed in the gas phase was suggested as highly controllable and flexible method,[79,80] albeit experimentally very sophisticated and much more "expensive" than PVD. The method allows, in principle, precise control over the cluster size. The latter is particularly important for studies in the so-called "non-scalable" regime of a gold particle size, where adding or removing only one gold atom to the cluster may considerably change its functional properties, e.g. catalytic performance.[81] Note, that using this cluster deposition one has to take precautions against coalescence of deposited clusters, which implies very low metal coverages.

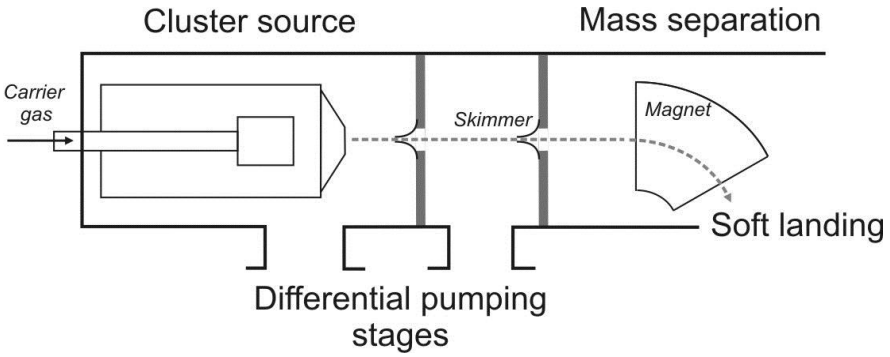

Figure 12.11. Schematic representation of a mass-selected cluster deposition. Mass separation employs deflection of charged gold clusters in an electric or magnetic field. Here, segmented magnet is only shown, for simplicity.

Basically, the apparatus includes a cluster beam source, a mass filter, and facilities for soft landing deposition (Fig. 12.11). In the beam source, a metal vapor is ejected into a flow of a cooled inert gas, where the condensation of a supersaturated vapor into clusters occurs. The metal vapor can be generated by laser ablation, sputtering, a pulsed or continuous arc, or thermally.[79,82] Depending on the type of source, the gas pressure inside the condensation zone ranges from a few millibar to a few bar. The cluster size distribution depends on the time till the mixture of carrier gas and clusters exits the aperture into the vacuum region, which can be controlled, for example, by the gas flow rate. The expansion accelerates the clusters, which, in the limit of large pressure drop

across the aperture ("free-jet expansion"), are thermally equilibrated with the bath gas and have the same velocity distribution irrespective of their size.

Mass separation and selection of the clusters is based on deflection of the charged species either in an electric or magnetic field. The Wien filter applies orthogonal electric and magnetic fields to charged particles. Therefore, the equipment additionally requires a cluster ionizer (except of sputtering-based beam sources which contain substantial amounts of charged species). Some cluster sources even employ two mass-filters: A high resolution instrument such as time-of-flight analyzer to measure the mass spectrum in the free beam, and a lower resolution high-throughput device to narrow the native mass distribution prior to deposition. Mass separation of neutral clusters is still challenging (for more details, see ref. [82,83]).

Soft-landing of clusters means that the clusters do not fragment upon collision with a substrate. The kinetic energy of clusters to fulfil this regime is typically set to 0.1 eV per atom. Following the well-known Maxwell-Boltzmann velocity (v) distribution function, i.e., $f(v) \sim (m/2\pi kT)^{3/2} v^2 exp(-mv^2/2kT)$, the soft-landing regime may be achieved by proper choosing the mass m and temperature T of a carrier gas. For example, for Ar at 100 K, the velocity at the peak of the distribution is about 200 m s^{-1}, which corresponds to the impact energy of an Au cluster about 0.04 eV/atom. However, in the case of He at 300 K as the carrier gas, this would yield 1.5 eV/atom that falls into the range of medium impact energies (1 - 10 eV/atom).[83] In addition, soft landing can be achieved by decelerating the charged clusters by electric field while approaching a support (see for example, refs. [84,85]).

Several experiments demonstrated that soft landing of metal clusters is possible, indeed.[81,86,87] STM characterization of Au_n^+ (n=1-8) clusters deposited on TiO_2(110) showed that, starting from dimers, Au_2^+, the clusters could be deposited intact, and no cluster agglomeration occurred, at least, at room temperature,[87] as shown in Fig. 12.12. Interestingly, single atom deposition (n=1) revealed no small Au clusters on surface (see Fig. 12.12a). These observations indicate that Au monomers are highly mobile on the TiO_2(110) surface, leading to aggregation into larger clusters, containing on the orders of tens of atoms, on average.

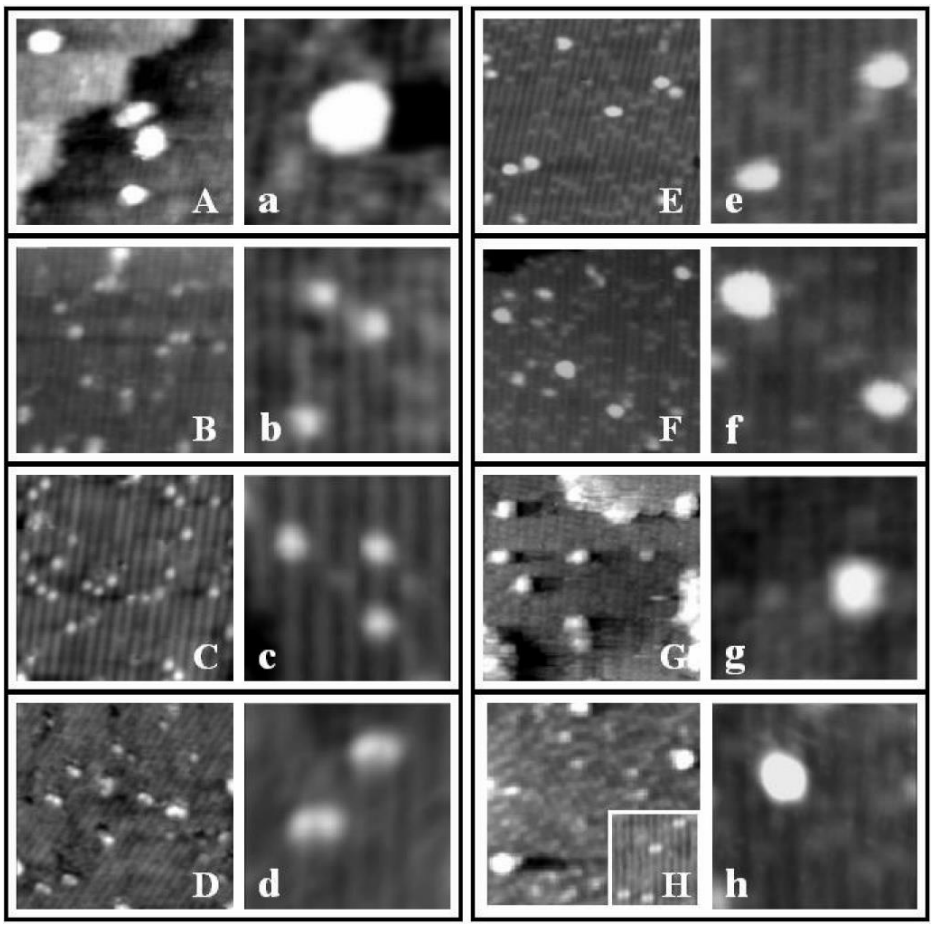

Figure 12.12. STM images 14 nm x 14 nm (uppercase letters) and 5 nm x 5 nm (lowcase letters) of Au_n^+ clusters deposited on TiO_2(110) at 300 K (n = 1 – 8 for (a - h), respectively). The bright protruding spots are the Au clusters, the dim spots between the rows of 6.5 A apart are bridging oxygen vacancies of TiO_2(110). (Reprinted with permission from Tong et al.[87]. Copyright (2005). American Chemical Society).

Finally, the deposition onto a thin buffer layer of rare gas [88] (typically Xe) formed on a substrate cooled down to cryogenic temperatures (ca 40 K) may also lead to the non-fragmented deposition of metal clusters. Subsequent heating to desorb the weakly bound buffer layer is accompanied by adsorption of the clusters onto a substrate.

In principle, mass-selected cluster deposition is not limited to the very small clusters. In fact, modern deposition sources can produce clusters up to ~ 70 000 atoms, depending on the target material. For example, $Au_{(923\pm23)}$ nanoclusters were produced using a magnetron-sputtering gas-condensation cluster beam source.[89] Characterization

of deposited "giant" Au clusters by ac-STEM showed the formation of icosahedral, decahedral, and face-centered cubic isomers (see Section 12.4) within a set of populations, with each population corresponding to a specific set of formation conditions. Tuning these conditions, one can eliminate completely all icosahedral clusters, which are commonly found under other conditions, thus providing a tool to the preparation of nanoclusters containing a dominant or single isomer.[90]

12.6.3. Reactive deposition methods

The *buffer layer assisted deposition* mentioned above was further extended to PVD of metals on "amorphous solid water" films or, simply saying, on ice formed by water adsorption on a planar substrate kept at temperatures below 130 K.[91] After metal deposition, the sample is heated to the room temperature to desorb weakly bound water molecules. The formation and aggregation of particles on ice films is a complex process that is driven by the dewetting, islanding and sublimation of ice on heating and is yet not well understood.[92] Nonetheless, water assisted deposition of gold on silica films showed that one can independently control particle size (in the range of several nanometers as observed) and only change particle density by repeating the whole deposition procedure.[93]

Chemical Vapor Deposition (CVD) is based on use of volatile complexes as precursors, which decompose on a target substrate kept at elevated temperatures. The CVD can be performed by direct sublimation of solid precursor in vacuum or in the carrier gas such as nitrogen or hydrogen, the latter is additionally used as the reducing agent. Some preparations include passing the carrier gas through the precursor solution ("bubbling").

Usually, the gold(I) and gold(III) precursors are organometallic compounds such as alkyl(phosphine)gold(I) and dimethylgold(III) β-diketonates and their derivatives. [94-97] In general, synthesis of the gold precursors is often very complex and shows a low yield. In addition, many precursors are light and/or air-sensitive, and as such are difficult to handle. Dimethylgold(III) carboxylates were recently suggested as viable precursors due to their sufficient volatility and thermal stability.[98]

The principal advantage of CVD over PVD is the possibility to uniformly cover rough and/or porous surfaces without having shade zones which are inevitable in PVD using a directional beam of the Au atoms.[95] However, the CVD method suffers from the lack of control of cleanliness arising from the stripping of the ligands and decomposition at surface. It is noteworthy, that this method is characterized by high deposition rates, thus resulting in granular films rather than isolated nanoparticles, and is, therefore, primarily aimed at deposition of gold thin films in microelectronics, metal coatings, etc. There are only few surface science studies on CVD-prepared gold nanoparticles. In particular, AFM measurements revealed significant sintering of Au particles on TiO_2(110) under an ambient atmosphere at temperatures as low as 363 K.[99] However, pre-treatment of the surface with ultraviolet radiation before CVD prevented particles agglomeration. It was suggested that such behaviour resulted from the presence of hydroxyl groups which formed as a result of photo-induced dissociation of adventitious water adsorbed on titania surface from residual gases in vacuum used (~ 10^{-6} mbar), since the titania surface is known to be active in water adsorption. It was proposed that the hydroxyl groups react strongly with the gold (I)-phosphine precursor used and thereby brought about the formation of highly stable small gold particles, which showed limited agglomeration even at 493 K in air.

12.6.4. Deposition from solution

Certainly, the planar supports in the form of thin films or single crystals are suited for gold deposition from solution as well, since such supports do not suffer from diffusion limitations associated with a porosity of real catalytic supports. For such deposition, one can, in principle, use the same procedures and treatments as described in Chapter 7 of this book. Again, gold nanoparticles can already be formed in solution and only need to be brought onto the support (reduction-deposition method), or the solution contains gold precursor to be thermally reduced at inorganic support (deposition-reduction method). To date, majority of such studies on planar supports utilizes the first approach. The surface science studies aimed at fundamental understanding of deposition-precipitation processes are, in essence, in the premature state (see ref. [100]).

Putting a few droplets of gold-containing solution onto the support and subsequent drying in ambient typically results in a non-uniform material distribution across the surface. To have it spatially more uniform, a *spin coating* technique is employed, i.e. a few droplets of solution is put on the center of the substrate, which is then rotated at certain speed in order to spread the material by centrifugal force. Another approach is dipping the substrate into the solution and pulling it slowly out, which is usually referred to as a dip-coating method.

12.6.5. Deposition of ordered particles

Recently, the deposition methods have been developed which aim at a simultaneous control over particle size as well as distance between the Au particles. The latter parameter may be important for gold application in photonics and sensors, and in catalysis of diffusion-controlled reactions. One such approach includes deposition of a monolayer of Au filled *micelles* (first prepared in solution, see also Chapter 6) with a different length of the polymeric ligand.[101]. The preparation allows deposition of Au particles of the mean particle size ranged between 1 and 15 nm with very narrow particle size distribution. The micelles can then be brought to the planar substrate by dip-coating.[101,102] The resulting systems revealed hexagonally arranged pattern of Au nano-dots, with the average distance between Au nanoparticles being controlled by the total length of the diblock copolymers (see Fig. 12.13). The nature of substrate seems not to play considerable role on particle spatial distribution.[101] Removing of the polymeric shell can be achieved by annealing in UHV or by treatment in oxygen plasma. However, this issue remains the most uncertain in these experiments.

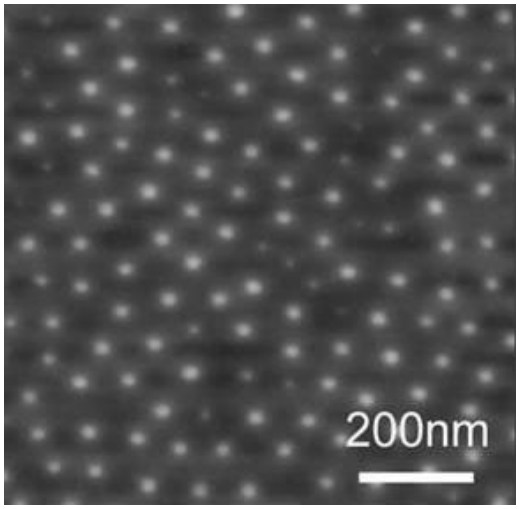

Figure 12.13. AFM image of gold nanoparticles deposited by dip-coating of inverse micelles on ultrathin TiC films (adapted from ref. [103]). The Au particles were synthesized using polystyrene-block-poly(2-vynilpyridine) as encapsulating agent. The mean particle height is around 2 nm. (Note, that the lateral size of the particles appears much larger than 2 nm due to the tip-sample deconvolution effects).

Another approach for ordering metal particles on surfaces employs *electron beam lithography* (EBL) for production of a patterned template followed by metal deposition using PVD, as nicely demonstrated first for Pd and Pt particles on various supports.[104-107] Briefly, a highly collimated electron beam is exposed to a thin layer of polymeric resist (such as poly(methylmethacrylate) spin-coated on a flat substrate (for example, a Si(100) wafer covered by the native oxide film or coated with thin film of alumina). The electron irradiation decomposes the polymer backbone, making it possible to dissolve the exposed polymer in a developing solution. Then a metal film is deposited on the surface by PVD, and the remaining polymer is removed with acetone. In the first experiments with Pt, the resulting systems showed highly ordered arrays of metallic particles about 30 nm in lateral size with 100 nm periodicity.[104]

Recently, a combined EBL and PVD preparation has been applied to gold, in particular for surface-enhanced Raman scattering (SERS) applications.[108] Using two different preparations (i.e. lift-off and plasma etching), a variety of nanostructures (disks, holes, gratings and other complex nanostructures) were fabricated. Large SERS

enhancement was observed which was dependent on the precise geometry of the nanostructures.

Note also, that the EBL was effectively used for substrate patterning and subsequent deposition of ligand protected gold particles, which selectively bound to the patterned substrate.[109] Another possibility is patterning of Langmuir-Blodgett films of colloidal gold.[110,111] More about nanolithography methods in application to gold can be found in the review [112].

To conclude this section, it is fair to say that the preferential choice in using one or another deposition method depends on many factors and is primarily determined by objectives of a study. On the one hand, all methods based on non-vacuum depositions have an inherent tendency to introduce contaminations into the system. On the other hand, the most clean, physical vapor and cluster depositions are hardly suited for preparations of technically relevant systems on large scale.

12.7. Surface Science Studies of Gold Nanoparticles

12.7.1 Nucleation and growth

Gold on a TiO_2(110) single crystal support is one of the most widely studied planar model system involving gold.[16-18] The (110) surface of TiO_2 rutile is the most stable surface consisting of alternating rows of titanium and oxygen atoms with half of the titanium atoms covered by so-called bridging oxygen. These oxygens are relatively weakly bound and can be removed upon high-temperature annealing (in order to form an electrically conducting support), ultimately creating oxygen vacancies, which can strongly influence the support's chemistry [113] (see also Fig. 12.12).

On the basis of electron and ion spectroscopy results, it was proposed that PVD-deposited gold at room temperature first grows on TiO_2(110) two-dimensionally (2D) at very low coverage, which then subsequently changes to three-dimensional (3D) growth with increasing coverage.[114,115] At higher deposition temperatures, the growth mode is more 3D from the onset, indicating that the 2D growth at low temperatures is a kinetically limited mode (see also below).[114-117] Very similar behaviour was later

observed for gold deposited on thin titania films grown on Ru(0001)[118] further supporting the concept that thin oxide films are, indeed, suitable supports for studying highly dispersed metal particles.

Early high resolution STM studies, corroborated by DFT calculations, showed direct relationship between gold particle nucleation and surface oxygen vacancies on TiO_2(110).[119] Further studies,[120] however, have revealed that the TiO_2(110) surface is very sensitive to the traces of water in the UHV background leading to the formation of surface hydroxyl (OH) groups, which likely have influenced previous studies on gold deposition on this support. Indeed, hydroxyls were found to promote gold sintering and strongly affect the particle size distribution.[121]

When gold was deposited on TiO_2(110) at 300 K and then annealed to 770 K the $(111)_{Au}//(110)_{TiO2}$ epitaxial relationship was observed, whereas deposition at 770 K preferentially gave rise to the $(112)_{Au}//(110)_{TiO2}$ epitaxy.[16,122] Interestingly, the Au lattice does not appear to undergo any deformation in spite of the minimal strain that must be overcome to match the TiO_2 epitaxy, indicating that the interaction between gold and titania is rather weak. On the other hand, the epitaxial relationship between titania and gold is strong enough, such that particles can grow in a Au(111) epitaxy up to rather large sizes.[16]

On CeO_2(111) thin films, at the lowest coverage, gold preferentially nucleated on terraces, presumably on point defects, e.g. oxygen vacancies, typical for ceria which is famous for its facile oxygen uptake and release behaviour. [123] At increasing gold coverage, particles are also formed at the step edges exposing a large variety of low-coordinated sites (Fig. 12.14a). Defects density on terraces could be increased considerably by high-temperature annealing in UHV. Gold deposition on this "reduced" surface resulted in the particles which were much smaller when compared to deposition of the same amount of gold on the fully oxidized ceria surface (see Fig. 12.14). Only at high coverage, the Au particles grew homogeneously on the flat CeO_2(111) terraces.[124] Gold exhibited a 3D growth mode from the onset resulting in nanoparticles, which were fairly stable towards sintering in vacuum at elevated temperatures. Increasing amounts of deposited gold essentially did not change the aspect (height/width) ratio of the particles, i.e. in agreement with thermodynamic considerations discussed in the Section 12.3.

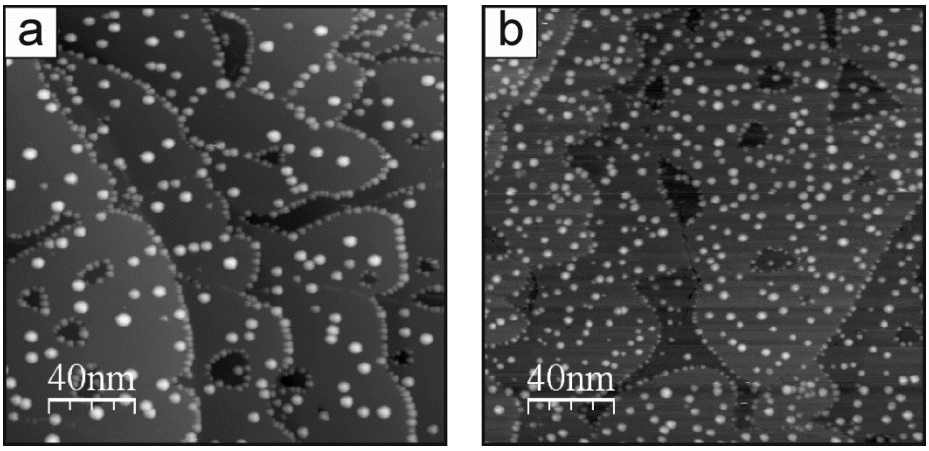

Figure 12.14. STM images of Au particles deposited on fully oxidized (a) and partially reduced (b) CeO_2(111) films grown on Ru(0001). For the latter, the fully oxidized film was annealed at 1000 K in UHV prior to the deposition of the same amount of gold as for image (a).

Surprisingly, gold deposited onto crystalline alumina thin films did not show preferential nucleation as previously observed for Pd and Ag on the same support. The hemi-spherical particles were found fairly randomly distributed on the surface.[125,126] Such a behavior has been attributed to the particular structure of the thin alumina film grown on NiAl(110) which results in strong interaction with the gold single atoms.[127]

In principle, one can derive the adhesion energy between a metal and a support, if the precise geometry of supported particles is known. For the hemi-spherical metal particles, mainly exposing (100) and (111) facets, and contacting a substrate via the (111) plane (see Fig. 12.15), an analysis leads to the following expression for the adhesion energy:[128]

$$W_{adh} = \gamma_{111}\left(2 - \frac{3}{\sqrt{2}}\frac{h}{w}\frac{s+1}{2s+1}\right) \qquad (4)$$

where γ_{111} is the surface energy of the (111) surface, h (w) is height (width) of particles; s is the ratio of top-facet side lengths (s_{100}/s_{111}).

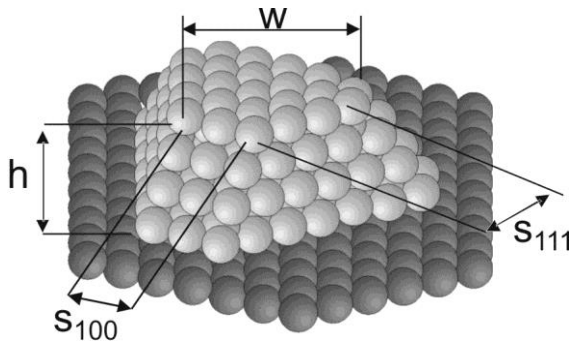

Figure 12.15. Structural characteristics used for deriving the adhesion energy between a metal particle and a support.

For example, STM images of annealed gold particles on a $Fe_3O_4(111)$ thin film showed [125] well-faceted particles, exhibiting mostly hexagonal shape of top facets as shown in Fig. 10b. In addition, the histogram analysis of STM images revealed that height of the particles was multiple of ~2.5 Å (which is close to the height of a monolayer of gold in the (111) orientation). All these findings suggest that particles grow by increasing the number of the atomic layers parallel to the surface. Although atomic resolution of the top facets was not achieved, it seems plausible that the top facets show up the (111) surface owing to small (~ 3 %) lattice mismatch between Au(111) and $Fe_3O_4(111)$ surfaces. Based on the structural parameters derived from STM and using the theoretical value of 1.28 J/m^2 for Au(111) as calculated by DFT,[129] eq. (4) yields 2.3 J/m^2 for the adhesion energy between Au and the iron oxide. For comparison, Pd particles and Pt particles deposited on the same support showed the energies of 3.1 J/m^2 and 3.8 J/m^2, respectively,[130] using the values of 1.92 J/m^2 for Pd(111) and 2.3 J/m^2 for Pt(111) from the same DFT calculations, for consistency.[129] It is evident that Au interacts with the iron oxide surface more weakly than do Pt and Pd.

In the above examples gold was deposited using PVD, which typically resulted in the mean particle size ca 2 - 5 nm, except deposition at cryogenic temperatures where limited surface diffusion leads to the stabilization of single Au ad-atoms or the formation of very small aggregates.[21,131,132] For the preparation of monodispersed Au particles below 1 nm in size, deposition of mass-selected clusters seems to be the only method (see Section 12.6.2). As mentioned above, the Au_n^+ (n=2-8) clusters, adsorbed on $TiO_2(110)$,

showed no cluster agglomeration at room temperature [87] (Fig. 12.12). In contrast, gold single atoms sintered rapidly and formed larger aggregates similarly to the samples prepared by PVD. In addition, the STM study revealed that supported Au_5 – Au_8 clusters all exhibited 3D- structures, albeit theory and gas-phase experiments indicated their planar configuration. These findings suggest that support, indeed, has certain stabilization effect on particular structures of gold clusters. Interestingly, no direct evidence was found in these experiments for oxygen vacancies on TiO_2 to be required for binding the mass-selected clusters. Basically, the same conclusion has been drawn after revision of previous STM results of PVD-deposited Au particles.[121]

The role of oxygen vacancies on the structure of gold clusters have been addressed using MgO(100) thin films.[81,133] Experimental and theoretical studies of mass-selected Au_8^+ clusters deposited on perfect and defect-rich MgO films revealed that the so-called colour (or F-) centres play a crucial role in the reactivity of gold clusters in CO oxidation. DFT analysis showed that, although the Au_8 cluster adsorbed on F-centre is only slightly distorted as compared to the gas phase neutral cluster, it binds much more stronger to the defect, and the charge transfer from the oxygen vacancy to the Au_8 cluster occurs, as observed by IR spectroscopy of CO as a probe molecule.[81] It should be pointed out noted that final charge state of (initially positively charged) mass-selected Au clusters is case-sensitive.

12.7.2 Particle size effects

The ability of the cluster deposition technique to vary a cluster size atom-by-atom allowed monitoring size dependent reactivity of the gold clusters, in particular in the CO oxidation. TPD and pulsed molecular beam studies of supported Au_n clusters revealed non-scalable activity towards CO_2 formation in such that clusters below Au_8 on MgO[81,133] (Fig. 12.16) and below Au_7 on TiO_2(110)[134,135] were essentially inert. At increasing cluster size some sort of oscillatory behaviour was obtained for reactivity (Fig. 16b). Another important observation, that came out from these studies, is structural flexibility (“fluxionality”[81]) of the gold-based systems, which seem to adopt the optimum structure in their response to the gas adsorption and the most favourable reaction pathway.

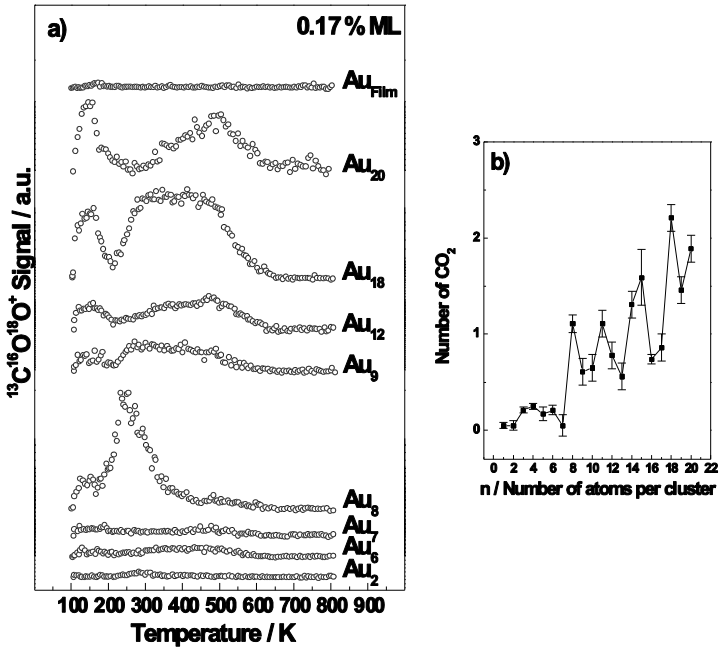

Figure 12.16. (a) TPD signal of $^{13}C^{16}O^{18}O$ production upon sequential adsorption of $^{18}O_2$ and ^{13}CO at 90 K on Au_n clusters deposited onto defect-rich MgO thin films. The reactivity of Au_n is expressed in (b) as the number of formed CO_2 molecules per cluster. (Reproduced with permission from Arenz et al. [81]. Copyright Wiley-VCH Verlag GmbH & Co. KGaA.)

Mass-selected Au clusters consisting of less than ten atoms were deposited on HOPG surfaces pre-sputtered by Ar+ ions in order to increase density of the defects acting as nucleation centers. [23] STM inspection of Au_7 clusters suggested the absence of sintering upon deposition.[136] Only Au_8 can be significantly oxidized using atomic oxygen source and subsequently reduced by CO, as revealed by XPS. The results were somewhat different for Au clusters deposited on thermally grown silica films on Si(111), thus indicating importance of metal-support interactions for reactivity of gold.

TPD and IRAS studies of CO adsorption on gold nanoparticles deposited onto various oxide supports clearly showed a particle size effect in that small particles adsorb CO more strongly. [125,137] At low Au coverages and low deposition temperatures, i.e. at the conditions providing the formation of small Au aggregates, CO was found desorbing at temperatures as high as 300 K. Such relatively strongly bound states have never been observed on Au single crystal surfaces[46,48,138,139] and, therefore, have been associated with highly uncoordinated gold atoms present on the surface of the

smallest particles.[137] However, these states disappear upon annealing to 400-500 K, which is accompanied by strong reduction of the CO uptake due to gold sintering, in full agreement with STM results pointing out low thermal stability of small gold clusters. Indeed, the spectra for annealed samples become very similar to those obtained on the stepped gold surfaces. Comparison of CO TPD spectra of gold deposited on various oxide supports showed that, for a given nanoparticle size, the interaction of CO with Au particles is essentially identical.[125] These findings suggest that the support effects frequently reported in the literature for real catalytic systems, particularly in oxidation reactions, could be associated with the oxide-dependent size distribution of gold nanoparticles and atomic structure of the gold/oxide interface, which are, in turn, controlled by defect structures of oxide supports. In addition, as mentioned above for the titania support, the presence of OH surface species either in the course of the catalyst preparation or under reaction conditions may also play a critical role in the support effects reported.

12.7.3 Environmental effects

Majority of studies on the Au model catalysts was conducted under well-controlled, but vacuum-compatible conditions. Relatively unexplored are potential modifications of these systems in a reactive environment at nearly atmospheric pressures. In this respect, many fundamental questions still remain, including the possibility of reaction induced morphological changes in the system. From general bond conservation considerations, a weakening of the Au-Au bonds within the cluster may occur when an Au cluster strongly interacts with the reactive gas, ultimately leading to a disruption of the structure of the metal particle. Also, adsorption induced reshaping of gold particles is predicted by DFT calculations of an Au_{79} cluster (~ 1 nm in diameter) reacting with CO.[140] The strength of interaction between the gold nanoparticle and the support may play a significant role in determining the stability of these systems under realistic pressures and temperatures. Although Au particle reshaping was experimentally proven on Au/MgO catalysts with the help of high-resolution electron microscopy,[141] *surface* studies of gold nanoparticles under realistic reaction conditions remain scarce. To some extent, this is due to the lesser number of techniques available in the field of surface science to carry

out experiments in ambient other than vacuum. Below, we show few examples of such studies in order to illustrate environmental effects on gold.

We first address to results obtained by STM which may operate, in essence, in any atmosphere if the sample is electrically conducting. For example, no morphological changes of the Au particles deposited on thin FeO(111) films were observed in oxygen and hydrogen environments at pressures up to 2 mbar at room temperature.[142] However, in CO and CO + O_2 (2:1) atmospheres, the destabilization of Au atoms located at the step edges was observed even at ~ 10^{-3} mbar leading to the formation of mobile Au species, which diffused across the surface. The results were rationalized in terms of a stronger interaction of gold with CO, as compared to O_2 and H_2, which significantly weakens the Au/support interaction for the smallest particles.

STM studies [143,144] of Au/TiO_2(110) revealed a form of Ostwald ripening (the growth of large particles at the expense of small particles) by exposing to 14 mbar of O_2 at 300 K. This process appeared to be even stronger in the stoichiometric mixture of O_2 and CO. Further *in situ* STM studies [144,145] revealed that an initial uniformly sized group of Au particles underwent severe Ostwald ripening at 450 K in 0.7 mbar of O_2. The presence of oxygen served to weaken Au-Au bonds, thereby promoting sintering. Note, however, that STM images taken under reaction conditions showed that the behavior of particles that were initially of the same size could be quite different, as some particles decreased in size or even disappeared, while others seemed to remain stable.

The morphology of the supported Au particles on CeO_2(111) films was studied by STM *in situ* and *ex situ* in CO, O_2 and CO + O_2 environment at room temperature.[124] No visible changes were observed after exposing Au particles to pure O_2 up to ~10 mbar. In the pure CO ambient, Ostwald ripening emerged above ~1 mbar. Meanwhile, sintering of the Au particles was observed in CO + O_2 (1:1) mixture at much lower pressure (~10^{-3} mbar) that mainly occurred along the step edges. The results indicate that the structural stability of the Au/CeO_2 surfaces is intimately connected with its reactivity in the CO oxidation reaction. The results revealed both similarities and differences with the Au/TiO_2(110)[145] and Au/FeO(111)[142] systems, suggesting that the oxide support is deeply involved in the stabilization of the supported Au nanoparticles.

To address the structure of adsorbed species on gold under reaction conditions, SFG technique seems to be well-suited, as it was nicely demonstrated for CO adsorption on Pd nanoparticles in the wide range of pressures. [146] Comparative studies of CO adsorption on pure and ion-sputtered gold surfaces by SFG [147] revealed the important role of the defect sites in the CO adsorption. In addition, a promoter such as iron oxide was found to enhance CO adsorption, which is believed to take place at the interface between gold and iron oxide. In addition, SFG was successfully applied to surfactant coated Au nanoparticles (~ 15 nm) deposited onto Si wafer [148]. Here, polar orientation and degree of conformational order of adsorbed surfactants could be addressed. Nonetheless, it is fair to say that the SFG studies on gold in catalytic reactions are scarce, indeed.

The instrumentation of synchrotron-based, ambient pressure XPS is much more sophisticated and hence costly, that in fact prevents this technique to be present in many laboratories. Recent *in situ* AP XPS studies [149,150] were particularly focused on interaction of gold with oxygen, which appears to be the most critical step in oxidation reactions on gold. The results showed that molecular oxygen does not oxidize Au at room temperature, either in the form of supported particles on TiO_2(110) or in bulk (foil) form at pressures of up to 1 Torr [149]. In addition, the experiments demonstrated that X-rays play a critical dual role during *in situ* measurements and that care must be taken to carry out experiments and interpret spectra, especially when using intense synchrotron radiation.

By using ozone as a more strongly oxidizing agent, the formation of a surface oxide on gold foil was monitored by AP XPS [150]. However, this phase was unstable and decomposed under vacuum and even in the presence of ozone, but at higher temperatures. It was found that the surface oxidation led to structural modifications of the gold surface which is accompanied by the formation of low-coordinated Au atoms.

12.8 Two-dimensional Gold

In the course of preparation of gold model catalysts on planar oxide supports, gold was frequently observed in form of islands consisting of just a single layer of atoms. In addition, STM studies combined with reactivity measurements of Au deposited onto a

TiO_2(110) single crystal and a titania thin film in the CO oxidation reaction in the mbar pressure range,[151-153] showed that maximum catalytic activity for these clusters coincides with the metal-to-semiconductor transition (determined by tunneling spectroscopy), which in turn coincides with a transition from 2D islands into 3D nanoparticles. Behind the general interest to the physics of low-dimensional materials, such observations resulted in a closer look on the atomic structure of two-dimensional gold as catalytically active species.

On ultra-thin MgO(001) films grown on Ag(001), gold first forms flat, single-layer islands which develop into a nearly complete wetting layer with increasing Au coverage (Fig. 12.17a).[154] Whereas the single-layer Au islands dominate the surface of oxide films of 2-3 monolayers (ML) in nominal thickness, 3D nanoparticles are only formed on 8 ML-thick MgO(001) films. Combined experimental and DFT studies showed that the formation of 2D gold in this system is primarily controlled by the charge transfer from the support through an oxide film. Gold tends to increase the contact area with the support, as this maximizes the charge transfer into the gold affinity levels. Interestingly, this charge is localized at the islands rim. The respective electronic states are able to store one extra electron per low-coordinated edge atom, and become filled up with transfer electrons although the island interior remains neutral. The charge localization in the low-coordinated, edge atoms suggests the 2D Au islands to be potentially active for adsorption and chemical reactions involving electron-accepting molecules.

Although the above presented complex metal-oxide-metal (Au-MgO-Ag) structures can hardly be implemented in the catalysis design right away, the concept of charge-mediated control of the gold particle shape can, in principle, be transferred to bulky oxide supports as well, providing a suitable charge source in the oxide lattice in a near-surface region. The latter can be achieved by doping of oxide by other cations, or it may even occur as a result of “self-doping” by a small amount of impurities usually present in oxide support materials. Following this idea, high-valence dopants may serve as charge donors and provide extra electrons in the same way as a metal-supported ultrathin oxide film. Accordingly, low-valence dopants will show acceptor character and hence accommodate electrons from suitable adsorbates. Therefore, donors in an oxide lattice will have a similar effect on the particle shape as a metal support underneath an ultrathin

oxide film. This concept has recently been validated for CaO(001) films grown on Mo(001). It was found by STM that, on the doped film, the gold spreads out into extended monolayer islands (Fig. 12.17b), while the 3D growth is observed on the non-doped surface.[155]

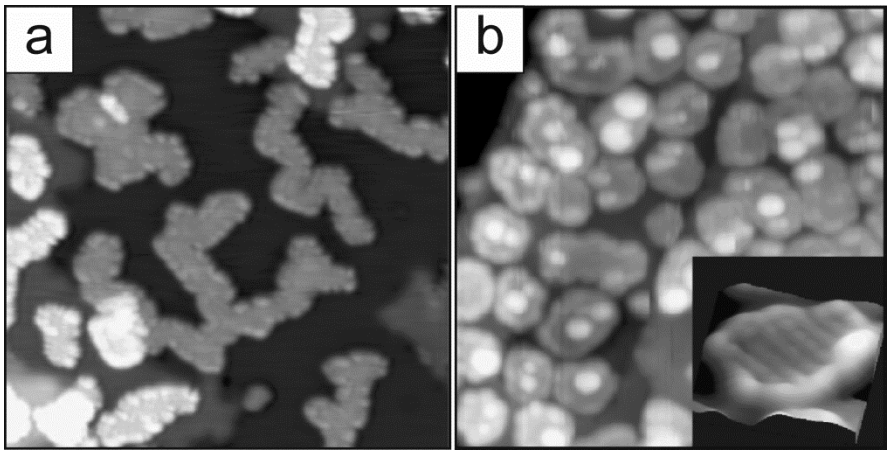

Figure 12.17. STM images of single-layer Au islands formed upon deposition of gold on 3 ML-thick MgO(001) film grown on Ag(001) (adapted from ref. [154]) (a) and Mo-doped, 10 ML-thick CaO(001) film grown on Mo(001) (adapted from ref. [155]) (b). Image sizes are 30 nm x 30 nm (a), and 50 nm x 50 nm (b). The inset in (b) shows a high-resolution image in perspective view that shows a stripe-like pattern on the Au surface, which is assigned to a Moiré structure formed between the square CaO(001) and the hexagonal Au(111) lattices.

12.9 Au-based Bimetallic Nanoparticles

Bimetallic nanoparticles often show synergy effects in that they exhibit properties distinct from those of mixture of monometallic particles.[156] In principle, bimetallic particles may form fully mixed alloys or a core-shell structure if, for example, composed of immiscible metals. Note again, that surface composition and hence atomic structures may deviate from those present in the bulk due to surface segregation, the degree of which depends on many parameters such as lattice mismatch, particle size, temperature, and ambient conditions. In this respect, Au-containing bimetallic systems received much attention on a theoretical ground by using *ab initio* calculations and Monte Carlo simulations.

As in the case of pure gold (Section 12.3), we first address general considerations applied to surface structures of bulky systems. Gold has much lower surface energies

when compared to other noble metals (Pt, Pd) and close to that of Ag, only.[157] Therefore, it is not totally surprising that even small concentration of Au in Pt results in a surface layer composed almost exclusively of Au, as judged by AES. [158] STM, LEED and LEISS measurements of a clean $Cu_3Au(100)$ surface, representing a classical ordering alloy, revealed an Au-rich terminated layer out of two possible surface terminations. [159]. For the $Au_3Pd(100)$ surface, STM with a so-called "chemical contrast" revealed the surface enriched by Au. [160] Figure 12.18 displays the high-resolution STM image where brighter protrusions are assigned to the surface Pd atoms, which are clearly at a much lower concentration when compared to the equilibrium distribution in the crystal bulk. In addition, ion scattering and tensor LEED analysis suggested that segregated topmost layer may have lattice constants different (in this case, smaller) from their respective bulk value.

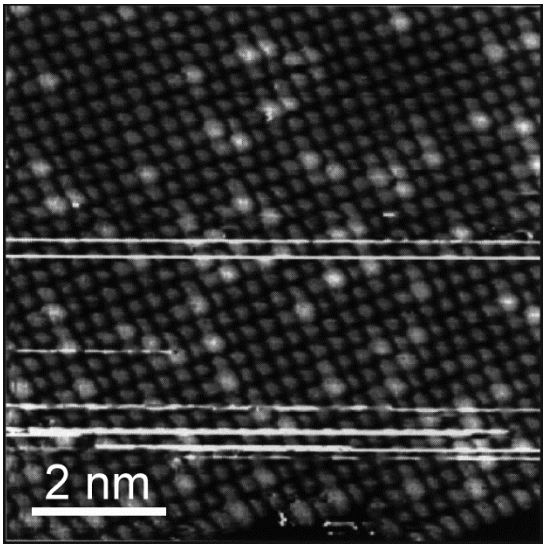

Figure 12.18. STM image of the clean $Au_3Pd(100)$ surface prepared by argon sputtering at 625 K. "White" atoms are palladium. (Adapted from ref. [160]). The streaks are due to the STM tip instability.

Basically, similar trend (Au segregation at surface) holds true also for bimetallic nanoparticles. Theoretical studies of both, 40 atoms [161] and 1654 atoms [157] Au-Pt clusters revealed an Au-shell and Pt-core structure as thermodynamically the most

favorable one. A strong surface Au enrichment was observed in all of the Au-Pt nanoparticles studied, [162] and the surface segregation of Au was more pronounced at increasing particle sizes.

On the other hand, Monte Carlo simulations of Au-Ag nanoparticles showed Ag rather than Au segregating at the surface. [163] (Note that the surface energies of Ag and Au crystals are very close.[157]) The surface segregation is composition, size, and temperature dependent. The surface Ag fractions are higher in the Ag-richer or larger-sized particles at low temperature. The resulting structures are formed upon the competition and balance between surface segregation and alloy formation. In addition, the calculated distribution of Au ensembles (e.g., monomers, dimers, trimers) on the particle surface depends on the Au:Ag compositional ratio and temperature. It is believed that metal surface distribution affects the reactivity and selectivity of bimetallic catalysts in structure sensitive reactions. As an example, acetoxylation of ethylene to vinyl acetate (VA) was found to be strongly promoted by adding gold into a Pd catalyst. Comparative studies of the Au(100) and Au(111) surfaces as a function of Pd coverage showed the enhanced rates of VA formation for low Pd coverages relative to high Pd coverages, which were assigned to the critical reaction site for VA synthesis consisting of two noncontiguous, suitably spaced, Pd monomers. [164] The role of Au is to isolate single Pd sites that facilitate the coupling of critical surface species to product, while inhibiting the formation of undesirable reaction by-products.

Certainly, the surface segregation may change substantially when the Au-based nanoparticles are exposed to the ambient containing oxidizing or reducing agent. In this case, the other metal usually having higher affinity for oxygen than gold will be prone to segregate to the surface. Such effect was theoretically predicted for the $Ag_3Pd(111)$ surface in an oxygen atmosphere.[165] Whereas a minimal segregation energy stabilizes Ag-terminated surface structures in UHV, the much stronger oxygen bonding favours increasingly Pd-rich terminations in atmospheres with higher oxygen content.

The experimental surface science study of bimetallic nanoparticles is not trivial, as most of the electron spectroscopy methods have surface sensitivity comparable with the particle size. More sensitive is low-energy ion scattering spectroscopy (LEISS) that, for instance, allowed to determine surface composition of the Au-Pd bimetallic particles

vapour-deposited onto silica films.[166] The results showed Au surface enrichment, indeed, as predicted by theory, although to the lower extent as compared to extended Au-Pd surfaces. More straightforward are using vibrational spectroscopy of probe molecules like CO, albeit such studies also need complementary theoretical input. As an example, inset in Figure 12.19 depicts the ν(CO) stretching region in IR spectrum of CO adsorbed on silica supported Au-Pt particles.[167] The observed two bands are assigned to CO adsorbed in Au and Pt atop sites, respectively. In contrast to CO on Au, atop CO on Pt showed a substantial shift as a function of Au concentration, assigned to the electronic effect.

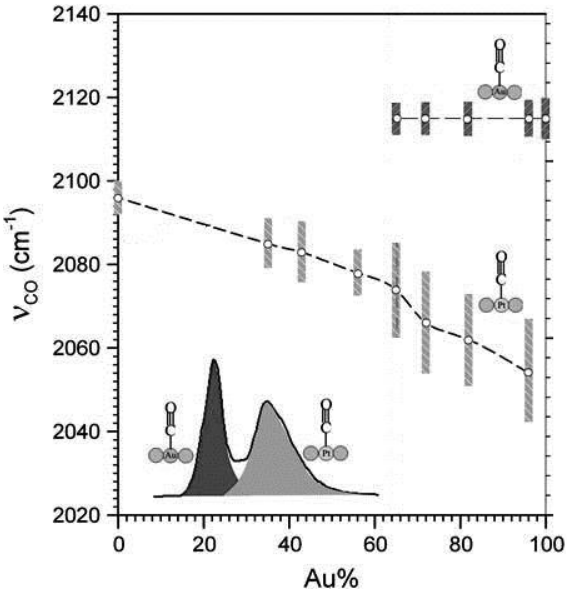

Figure 12.19. CO stretching frequencies of the two bands, assigned to terminal CO on Au and Pt atop sites (see inset), as a function of Au concentration in the Au-Pt nanoparticles. (Adapted from ref. [167]). The bars represent the peak width at half maximum.

Concluding remarks

In this Chapter, we addressed surface structures of gold. Surface science studies, using state-of-the-art surface-sensitive techniques, applied to well-defined model planar systems allow one to rationalize chemical and catalytic properties of gold nanoparticles which are very distinct from their bulky counterparts. In particular, it appears that the

(oxide) support plays the critical role in stabilizing atomic configuration, charge states and electronic structure of the ultra-small Au aggregates. The approach also allows monitoring the particle size effects as well as the effects caused by ambient conditions. The *in situ* experiments remain highly demanding for elucidating the reaction mechanisms.

Acknowledgements. I would like to thank all my co-workers, which names appear in the references below, for their tremendous work in the laboratories of the group Structure and Reactivity in the Department of Chemical Physics of the Fritz-Haber Institute (Berlin) head by Prof. Hans-Joachim Freund.

References

[1] M. Haruta, The Chemical Record 3 (2003) 75.
[2] M. Haruta, Gold Bull 37 (2004) 27.
[3] A.S.K. Hashmi, G.J. Hutchings, Angewandte Chemie International Edition 45 (2006) 7896.
[4] M.C. Kung, R.J. Davis, H.H. Kung, The Journal of Physical Chemistry C 111 (2007) 11767.
[5] G.C. Bond, C. Louis, D.T. Thompson, Catalysis by Gold, Imperial College Press, London, 2006.
[6] D.W. Goodman, Surface Review and Letters 02 (1995) 9.
[7] D.W. Goodman, The Journal of Physical Chemistry 100 (1996) 13090.
[8] H.-J. Freund, Angewandte Chemie International Edition in English 36 (1997) 452.
[9] C.T. Campbell, Surface Science Reports 27 (1997) 1.
[10] P.L.J. Gunter, J.W. Niemantsverdriet, F.H. Ribeiro, G.A. Somorjai, Catalysis Reviews 39 (1997) 77.
[11] C.R. Henry, Surface Science Reports 31 (1998) 231.
[12] D.R. Rainer, D.W. Goodman, Journal of Molecular Catalysis A: Chemical 131 (1998) 259.
[13] M. Bäumer, H.-J. Freund, Progress in Surface Science 61 (1999) 127.
[14] H.-J. Freund, Surface Science 500 (2002) 271.
[15] H.-J. Freund, G. Pacchioni, Chem. Soc. Rev. 37 (2008) 2224.
[16] F. Cosandey, T.E. Madey, Surface Review and Letters 08 (2001) 73.
[17] R. Meyer, C. Lemire, S.K. Shaikhutdinov, H.J. Freund, Gold Bull 37 (2004) 72.
[18] M. Chen, D.W. Goodman, Accounts of Chemical Research 39 (2006) 739.
[19] B.K. Min, C.M. Friend, Chemical Reviews 107 (2007) 2709.
[20] J.A. Rodriguez, S. Ma, P. Liu, J. Hrbek, J. Evans, M. Pérez, Science 318 (2007) 1757.
[21] T. Risse, S. Shaikhutdinov, N. Nilius, M. Sterrer, H.-J. Freund, Accounts of Chemical Research 41 (2008) 949.
[22] J. Gong, C.B. Mullins, Accounts of Chemical Research 42 (2009) 1063.
[23] D.-C. Lim, C.-C. Hwang, G. Gantefor, Y.D. Kim, Physical Chemistry Chemical Physics 12 (2010) 15172.
[24] J. Libuda, H.J. Freund, Surface Science Reports 57 (2005) 157.
[25] G.A. Somorjai, Applied Surface Science 121–122 (1997) 1.
[26] G. Rupprechter, Catalysis Today 126 (2007) 3.
[27] D.C. Meier, D.W. Goodman, Journal of the American Chemical Society 126 (2004) 1892.
[28] B.M. Hendriksen, S. Bobaru, J.M. Frenken, Topics in Catalysis 36 (2005) 43.
[29] D.C. Tang, K.S. Hwang, M. Salmeron, G.A. Somorjai, The Journal of Physical Chemistry B 108 (2004) 13300.
[30] M. Salmeron, R. Schlögl, Surface Science Reports 63 (2008) 169.

[31] J.V. Barth, H. Brune, G. Ertl, R.J. Behm, Physical Review B 42 (1990) 9307.
[32] M.A. Van Hove, R.J. Koestner, P.C. Stair, J.P. Bibérian, L.L. Kesmodel, I. BartoŠ, G.A. Somorjai, Surface Science 103 (1981) 189.
[33] U. Harten, A.M. Lahee, J.P. Toennies, C. Wöll, Physical Review Letters 54 (1985) 2619.
[34] V. Heine, L.D. Marks, Surface Science 165 (1986) 65.
[35] J.K. Gimzewski, R. Berndt, R.R. Schlittler, Physical Review B 45 (1992) 6844.
[36]
[37] D.G. Fedak, N.A. Gjostein, Acta Metallurgica 15 (1967) 827.
[38] D.G. Fedak, N.A. Gjostein, Surface Science 8 (1967) 77.
[39] H. Melle, E. Menzel, Superstructures on Spherical Gold Crystals, Zeitschrift für Naturforschung A, 1978, p. 282.
[40] K. Yamazaki, K. Takayanagi, Y. Tanishiro, K. Yagi, Surface Science 199 (1988) 595.
[41] N. Wang, Y. Uchida, G. Lehmpfuhl, Surface Science 284 (1993) L419.
[42] T. Kunio, T. Yasumasa, K. Kunio, A. Kazuhiro, Y. Katsumichi, Japanese Journal of Applied Physics 26 (1987) L957.
[43] A.R. Sandy, S.G.J. Mochrie, D.M. Zehner, K.G. Huang, D. Gibbs, Physical Review B 43 (1991) 4667.
[44] K.F. Peters, P. Steadman, H. Isern, J. Alvarez, S. Ferrer, Surface Science 467 (2000) 10.
[45] Y. Jugnet, F.J. Cadete Santos Aires, C. Deranlot, L. Piccolo, J.C. Bertolini, Surface Science 521 (2002) L639.
[46] C. Ruggiero, P. Hollins, Surface Science 377–379 (1997) 583.
[47] M. Borbonus, R. Koch, O. Haase, K.H. Rieder, Surface Science 249 (1991) L317.
[48] C.J. Weststrate, E. Lundgren, J.N. Andersen, E.D.L. Rienks, A.C. Gluhoi, J.W. Bakker, I.M.N. Groot, B.E. Nieuwenhuys, Surface Science 603 (2009) 2152.
[49] G. Wulff, Zur Frage der Geschwindigkeit des Wachsthums und der Auflösung der Krystallflächen, Zeitschrift für Kristallographie, 1901, p. 449.
[50] W.L. Winterbottom, Acta Metallurgica 15 (1967) 303.
[51] L.D. Marks, Reports on Progress in Physics 57 (1994) 603.
[52] C.L. Cleveland, U. Landman, T.G. Schaaff, M.N. Shafigullin, P.W. Stephens, R.L. Whetten, Physical Review Letters 79 (1997) 1873.
[53] J.A. Ascencio, M. Pérez, M. José-Yacamán, Surface Science 447 (2000) 73.
[54] C.L. Cleveland, U. Landman, The Journal of Chemical Physics 94 (1991) 7376.
[55] P.M. Ajayan, L.D. Marks, Physical Review Letters 63 (1989) 279.
[56] M. Mitome, Y. Tanishiro, K. Takayanagi, Z Phys D - Atoms, Molecules and Clusters 12 (1989) 45.
[57] S. Giorgio, C. Chapon, C.R. Henry, G. Nihoul, J.M. Penisson, Philosophical Magazine A 64 (1991) 87.
[58] T. Kizuka, N. Tanaka, Physical Review B 56 (1997) R10079.
[59] J. Liu, ChemCatChem 3 (2011) 934.
[60] Y. Han, R. Ferrando, Z.Y. Li, The Journal of Physical Chemistry Letters 5 (2014) 131.
[61] P. Hollins, Encyclopedia of Analytical Chemistry, John Wiley & Sons, Ltd, 2006.
[62] S.A. Chambers, Surface Science Reports 39 (2000) 105.
[63] W. Weiss, W. Ranke, Progress in Surface Science 70 (2002) 1.
[64] J.G. Chen, J.E. Crowell, J.T. Yates Jr, Surface Science 185 (1987) 373.
[65] F. Rochet, S. Rigo, M. Froment, C. d'Anterroches, C. Maillot, H. Roulet, G. Dufour, Advances in Physics 35 (1986) 237.
[66] M. Bäumer, D. Cappus, H. Kuhlenbeck, H.J. Freund, G. Wilhelmi, A. Brodde, H. Neddermeye, Surface Science 253 (1991) 116.
[67] R. Rohr, M. Bäumer, H.J. Freund, J.A. Mejias, V. Staemmler, S. Müller, L. Hammer, K. Heinz, Surface Science 389 (1997) 391.
[68] R.M. Jaeger, H. Kuhlenbeck, H.J. Freund, M. Wuttig, W. Hoffmann, R. Franchy, H. Ibach, Surface Science 259 (1991) 235.
[69] R. Franchy, J. Masuch, P. Gassmann, Applied Surface Science 93 (1996) 317.
[70] C. Becker, J. Kandler, H. Raaf, R. Linke, T. Pelster, M. Dräger, M. Tanemura, K. Wandelt, Journal of Vacuum Science & Technology A 16 (1998) 1000.

[71] J. Wollschläger, J. Viernow, C. Tegenkamp, D. Erdös, K.M. Schröder, H. Pfnür, Applied Surface Science 142 (1999) 129.
[72] D.R. Mullins, P.V. Radulovic, S.H. Overbury, Surface Science 429 (1999) 186.
[73] J.L. Lu, H.J. Gao, S. Shaikhutdinov, H.J. Freund, Surface Science 600 (2006) 5004.
[74] S. Surnev, M.G. Ramsey, F.P. Netzer, Progress in Surface Science 73 (2003) 117.
[75] S. Guimond, J.M. Sturm, D. Göbke, Y. Romanyshyn, M. Naschitzki, H. Kuhlenbeck, H.-J. Freund, The Journal of Physical Chemistry C 112 (2008) 11835.
[76] D. Löffler, J.J. Uhlrich, M. Baron, B. Yang, X. Yu, L. Lichtenstein, L. Heinke, C. Büchner, M. Heyde, S. Shaikhutdinov, H.J. Freund, R. Włodarczyk, M. Sierka, J. Sauer, Physical Review Letters 105 (2010) 146104.
[77] H. Hövel, I. Barke, Progress in Surface Science 81 (2006) 53.
[78] D.R. Frankl, J.A. Venables, Advances in Physics 19 (1970) 409.
[79] P. Milani, S. Iannotta, Cluster Beam Synthesis of Nanostructured Materials, Springer-Verlag Berlin Heidelberg, 1999.
[80] K. Wegner, P. Piseri, H.V. Tafreshi, P. Milani, Journal of Physics D: Applied Physics 39 (2006) R439.
[81] M. Arenz, U. Landman, U. Heiz, ChemPhysChem 7 (2006) 1871.
[82] C. Binns, Surface Science Reports 44 (2001) 1.
[83] C. Binns, in: J.A. Blackman (Ed.), Handbook of Metal Physics, Elsevier, 2008, p. 49.
[84] H. Haberland, M. Mall, M. Moseler, Y. Qiang, T. Reiners, Y. Thurner, Journal of Vacuum Science & Technology A 12 (1994) 2925.
[85] D.A. Eastham, B. Hamilton, P.M. Denby, Nanotechnology 13 (2002) 51.
[86] K. Bromann, H. Brune, C. Félix, W. Harbich, R. Monot, J. Buttet, K. Kern, Surface Science 377–379 (1997) 1051.
[87] X. Tong, L. Benz, P. Kemper, H. Metiu, M.T. Bowers, S.K. Buratto, Journal of the American Chemical Society 127 (2005) 13516.
[88] L. Huang, S.J. Chey, J.H. Weaver, Physical Review Letters 80 (1998) 4095.
[89] S. Pratontep, S.J. Carroll, C. Xirouchaki, M. Streun, R.E. Palmer, Review of Scientific Instruments 76 (2005) 045103.
[90] S.R. Plant, L. Cao, R.E. Palmer, Journal of the American Chemical Society 136 (2014) 7559.
[91] E. Gross, Y. Horowitz, M. Asscher, Langmuir 21 (2005) 8892.
[92] J.S. Palmer, S. Sivaramakrishnan, P.S. Waggoner, J.H. Weaver, Surface Science 602 (2008) 2278.
[93] E. Gross, M. Asscher, M. Lundwall, D.W. Goodman, The Journal of Physical Chemistry C 111 (2007) 16197.
[94] T.H. Baum, C.R. Jones, Journal of Vacuum Science & Technology B 4 (1986) 1187.
[95] E. Feurer, H. Suhr, Appl. Phys. A 44 (1987) 171.
[96] E. Szłyk, P. Piszczek, I. Łakomska, A. Grodzicki, J. Szatkowski, T. Błaszczyk, Chemical Vapor Deposition 6 (2000) 105.
[97] P.D. Tran, P. Doppelt, Journal of The Electrochemical Society 154 (2007) D520.
[98] A.A. Bessonov, N.B. Morozova, N.V. Gelfond, P.P. Semyannikov, S.V. Trubin, Y.V. Shevtsov, Y.V. Shubin, I.K. Igumenov, Surface and Coatings Technology 201 (2007) 9099.
[99] K.-i. Fukui, S. Sugiyama, Y. Iwasawa, Physical Chemistry Chemical Physics 3 (2001) 3871.
[100] M. Sterrer, H.-J. Freund, Catalysis Letters 143 (2013) 375.
[101] G. Kästle, H.G. Boyen, F. Weigl, G. Lengl, T. Herzog, P. Ziemann, S. Riethmüller, O. Mayer, C. Hartmann, J.P. Spatz, M. Möller, M. Ozawa, F. Banhart, M.G. Garnier, P. Oelhafen, Advanced Functional Materials 13 (2003) 853.
[102] B.R. Cuenya, S.-H. Baeck, T.F. Jaramillo, E.W. McFarland, Journal of the American Chemical Society 125 (2003) 12928.
[103] L. Ono, B. Roldán-Cuenya, Catalysis Letters 113 (2007) 86.
[104] A. Eppler, J. Zhu, E. Anderson, G. Somorjai, Topics in Catalysis 13 (2000) 33.
[105] J. Grunes, J. Zhu, M. Yang, G. Somorjai, Catalysis Letters 86 (2003) 157.
[106] S. Johansson, E. Fridell, B. Kasemo, Journal of Catalysis 200 (2001) 370.
[107] K. Wong, S. Johansson, B. Kasemo, Faraday Discussions 105 (1996) 237.
[108] Y. Weisheng, W. Zhihong, Y. Yang, C. Longqing, S. Ahad, W. Kimchong, W. Xianbin, Journal of Micromechanics and Microengineering 22 (2012) 125007.

[109] P.M. Mendes, S. Jacke, K. Critchley, J. Plaza, Y. Chen, K. Nikitin, R.E. Palmer, J.A. Preece, S.D. Evans, D. Fitzmaurice, Langmuir 20 (2004) 3766.
[110] M.H.V. Werts, M. Lambert, J.-P. Bourgoin, M. Brust, Nano Letters 2 (2002) 43.
[111] M.-V. Meli, R.B. Lennox, Langmuir 19 (2003) 9097.
[112] N. Stokes, A. McDonagh, M. Cortie, Gold Bull 40 (2007) 310.
[113] U. Diebold, Surface Science Reports 48 (2003) 53.
[114] L. Zhang, R. Persaud, T.E. Madey, Physical Review B 56 (1997) 10549.
[115] S.C. Parker, A.W. Grant, V.A. Bondzie, C.T. Campbell, Surface Science 441 (1999) 10.
[116] K.S. Ashok, K. Andrei, Y. Fan, D.W. Goodman, Japanese Journal of Applied Physics 42 (2003) 4795.
[117] N. Spiridis, J. Haber, J. Korecki, Vacuum 63 (2001) 99.
[118] T. Diemant, H. Hartmann, J. Bansmann, R.J. Behm, Journal of Catalysis 252 (2007) 171.
[119] E. Wahlström, N. Lopez, R. Schaub, P. Thostrup, A. Rønnau, C. Africh, E. Lægsgaard, J.K. Nørskov, F. Besenbacher, Physical Review Letters 90 (2003) 026101.
[120] O. Bikondoa, C.L. Pang, R. Ithnin, C.A. Muryn, H. Onishi, G. Thornton, Nat Mater 5 (2006) 189.
[121] D. Matthey, J.G. Wang, S. Wendt, J. Matthiesen, R. Schaub, E. Lægsgaard, B. Hammer, F. Besenbacher, Science 315 (2007) 1692.
[122] F. Cosandey, L. Zhang, T.E. Madey, Surface Science 474 (2001) 1.
[123] M. Baron, O. Bondarchuk, D. Stacchiola, S. Shaikhutdinov, H.J. Freund, The Journal of Physical Chemistry C 113 (2009) 6042.
[124] J.L. Lu, H.J. Gao, S. Shaikhutdinov, H.J. Freund, Catalysis Letters 114 (2007) 8.
[125] S.K. Shaikhutdinov, R. Meyer, M. Naschitzki, M. Bäumer, H.J. Freund, Catalysis Letters 86 (2003) 211.
[126] C. Winkler, A. Carew, R. Raval, J. Ledieu, R. McGrath, Surface Review and Letters 08 (2001) 693.
[127] N. Nilius, M.V. Ganduglia-Pirovano, V. Brázdová, M. Kulawik, J. Sauer, H.J. Freund, Physical Review Letters 100 (2008) 096802.
[128] K.H. Hansen, T. Worren, S. Stempel, E. Lægsgaard, M. Bäumer, H.J. Freund, F. Besenbacher, I. Stensgaard, Physical Review Letters 83 (1999) 4120.
[129] L. Vitos, A.V. Ruban, H.L. Skriver, J. Kollár, Surface Science 411 (1998) 186.
[130] Z.H. Qin, M. Lewandowski, Y.N. Sun, S. Shaikhutdinov, H.J. Freund, The Journal of Physical Chemistry C 112 (2008) 10209.
[131] M. Yulikov, M. Sterrer, M. Heyde, H.-P. Rust, T. Risse, H.-J. Freund, G. Pacchioni, A. Scagnelli, Physical Review Letters 96 (2006) 146804.
[132] H.M. Benia, X. Lin, H.J. Gao, N. Nilius, H.J. Freund, The Journal of Physical Chemistry C 111 (2007) 10528.
[133] A. Sanchez, S. Abbet, U. Heiz, W.D. Schneider, H. Häkkinen, R.N. Barnett, U. Landman, The Journal of Physical Chemistry A 103 (1999) 9573.
[134] S. Lee, C. Fan, T. Wu, S.L. Anderson, The Journal of Physical Chemistry B 109 (2005) 11340.
[135] S. Lee, C. Fan, T. Wu, S.L. Anderson, Journal of the American Chemical Society 126 (2004) 5682.
[136] D.C. Lim, R. Dietsche, M. Bubek, T. Ketterer, G. Ganteför, Y.D. Kim, Chemical Physics Letters 439 (2007) 364.
[137] C. Lemire, R. Meyer, S.K. Shaikhutdinov, H.J. Freund, Surface Science 552 (2004) 27.
[138] D.A. Outka, R.J. Madix, Surface Science 179 (1987) 351.
[139] J.M. Gottfried, K.J. Schmidt, S.L.M. Schroeder, K. Christmann, Surface Science 536 (2003) 206.
[140] K.P. McKenna, A.L. Shluger, The Journal of Physical Chemistry C 111 (2007) 18848.
[141] S. Giorgio, M. Cabié, C.R. Henry, Gold Bull 41 (2008) 167.
[142] D. Starr, S. Shaikhutdinov, H.-J. Freund, Topics in Catalysis 36 (2005) 33.
[143] X. Lai, D.W. Goodman, Journal of Molecular Catalysis A: Chemical 162 (2000) 33.
[144] A. Kolmakov, D.W. Goodman, Catalysis Letters 70 (2000) 93.
[145] A. Kolmakov, D.W. Goodman, Surface Science 490 (2001) L597.
[146] T. Dellwig, G. Rupprechter, H. Unterhalt, H.J. Freund, Physical Review Letters 85 (2000) 776.
[147] O. Hakkel, Z. Pászti, A. Berkó, K. Frey, L. Guczi, Catalysis Today 158 (2010) 63.
[148] T. Kawai, D.J. Neivandt, P.B. Davies, Journal of the American Chemical Society 122 (2000) 12031.

[149] P. Jiang, S. Porsgaard, F. Borondics, M. Köber, A. Caballero, H. Bluhm, F. Besenbacher, M. Salmeron, Journal of the American Chemical Society 132 (2010) 2858.
[150] A.Y. Klyushin, T.C.R. Rocha, M. Havecker, A. Knop-Gericke, R. Schlogl, Physical Chemistry Chemical Physics 16 (2014) 7881.
[151] X. Lai, T.P.S. Clair, M. Valden, D.W. Goodman, Progress in Surface Science 59 (1998) 25.
[152] M. Valden, X. Lai, D.W. Goodman, Science 281 (1998) 1647.
[153] M. Valden, S. Pak, X. Lai, D.W. Goodman, Catalysis Letters 56 (1998) 7.
[154] M. Sterrer, T. Risse, M. Heyde, H.-P. Rust, H.-J. Freund, Physical Review Letters 98 (2007) 206103.
[155] X. Shao, S. Prada, L. Giordano, G. Pacchioni, N. Nilius, H.-J. Freund, Angewandte Chemie International Edition 50 (2011) 11525.
[156] R. Ferrando, J. Jellinek, R.L. Johnston, Chemical Reviews 108 (2008) 845.
[157] K. Yun, Y.-H. Cho, P.-R. Cha, J. Lee, H.-S. Nam, J.S. Oh, J.-H. Choi, S.-C. Lee, Acta Materialia 60 (2012) 4908.
[158] S.E. Hörnström, L.I. Johansson, A. Flodström, Applied Surface Science 26 (1986) 27.
[159] H. Niehus, C. Achete, Surface Science 289 (1993) 19.
[160] M. Aschoff, S. Speller, J. Kuntze, W. Heiland, E. Platzgummer, M. Schmid, P. Varga, B. Baretzky, Surface Science 415 (1998) L1051.
[161] D.T. Tran, R.L. Johnston, Proceedings of the Royal Society of London A: Mathematical, Physical and Engineering Sciences 467 (2011) 2004.
[162] L. Deng, W. Hu, H. Deng, S. Xiao, The Journal of Physical Chemistry C 114 (2010) 11026.
[163] L. Deng, W. Hu, H. Deng, S. Xiao, J. Tang, The Journal of Physical Chemistry C 115 (2011) 11355.
[164] M. Chen, D. Kumar, C.-W. Yi, D.W. Goodman, Science 310 (2005) 291.
[165] J.R. Kitchin, K. Reuter, M. Scheffler, Physical Review B 77 (2008) 075437.
[166] K. Luo, T. Wei, C.W. Yi, S. Axnanda, D.W. Goodman, The Journal of Physical Chemistry B 109 (2005) 23517.
[167] D. Mott, J. Luo, A. Smith, P.N. Njoki, L. Wang, C.-J. Zhong, Nanoscale Research Letters 2 (2007) 12.